p-ISSN 2089 – 0133 e-ISSN 2477-6416
URL : https://jurnal.uns.ac.id/ijap/article/view/106099

DOI : https://doi.org/10.13057/ijap.v16i1.106099

THERMODYNAMIC ANALYSIS OF QUANTUM OTTO ENGINES: EXPLORING QUBIT EFFICIENCY IN NON-EQUILIBRIUM ENVIRONMENTS

Jeolous Malamula Nyasulu[1,2*], Chunyang Wang [2*], Zengxuan Zhao[1], and Mushtaq Rana Imran[1,3]
[1]Institute of Theoretical Physics, School of Physics and Optoelectronic Engineering, Ludong University, Yantai, 264025, China
[2]Domasi College of Education, Department of Physics, University of Malawi, Zomba, 305200, Malawi
[3]School of Science, Harbin Institute of Technology, Shenzhen, 518055, China
*jnyasulu688@gmail.com

Received 2025-15-07, Revised 2025-08-29, Accepted 2025-03-13,
Available Online, Published Regularly, April 2026

ABSTRACT

This paper presents an analysis of quantum Otto heat engines operating out of equilibrium. It explores the fundamental thermodynamic principles governing these engines, focusing on efficiency, work output, and the impact of environmental factors, including thermal gradients, external fields, noise, and decoherence. The study investigates the effects of non-equilibrium conditions on engine performance, highlighting challenges and opportunities in practical realizations. Through numerical simulations, the article examines the power, efficiency, and performance coefficients, revealing trade-offs between these metrics and the influence of temperature differences and internal coupling strength. The results demonstrate that non-equilibrium effects can significantly reduce efficiency compared to idealized scenarios, underscoring the importance of accounting for both quantum effects and real-world constraints in the design and optimization of quantum heat engines. This work contributes to the growing body of knowledge in quantum thermodynamics, offering insights for quantum computing, sustainable energy technologies, and thermodynamic cycles at the quantum scale.
Keywords**:** Quantum Otto heat engines; non-equilibrium environments; efficiency; work output; numerical simulations

INTRODUCTION

In recent years, the field of quantum thermodynamics has garnered significant attention [1], as researchers aim to understand and harness the principles of thermodynamics within quantum systems. Quantum Otto heat engines, inspired by the classical Otto cycle, have

1

2

emerged as a fundamental model to examine how quantum properties can be utilized for efficient energy conversion [2],[3]. These heat engines operate on the principles of thermodynamic cycles that consist of adiabatic and isochoric processes, providing an exciting platform for exploring the intricate interplay between quantum mechanics and thermodynamic efficiency [4].

Considering the validity of previous findings, single-qubit quantum Otto heat engines represent a vital area of research, demonstrating how the unique properties of quantum bits (qubits) can enhance engine performance. Using quantum phenomena such as superposition and coherence, these engines were expected to offer improved efficiencies compared to classical thermodynamic systems [5],[6]. However, operating in real-world conditions often involves interacting with non-equilibrium environments, where thermal fluctuations and noise can significantly impact the behavior and performance of quantum systems [7]. Understanding how single-qubit engines respond to these non-equilibrium conditions is crucial for optimizing their efficiency and functionality.

In addition to single-qubit systems, the analysis of quantum Otto heat engines presents a compelling frontier in quantum thermodynamics. These qubits enable the exploration of collective behaviors and correlations that can further enhance the thermodynamic performance of these engines [8–10]. Interactions between qubits may lead to shared quantum states, facilitating more effective energy transfer and extraction. This collective dynamism can potentially mitigate the detrimental effects of decoherence associated with individual qubit systems, offering new pathways to improve the efficiency of quantum heat engines operating under non-equilibrium conditions [11].

This paper aims to provide an analysis of single-qubit quantum Otto heat engines within non-equilibrium conditions, under the assumption of the theoretical and experimental frameworks [12]. We examined the fundamental thermodynamic principles that govern the operation of these engines, focusing on efficiency, work output, and the impact of various environmental factors. By exploring the implications of non-equilibrium conditions, including thermal gradients, interaction with external fields, and the influence of noise and decoherence, we seek to illuminate the challenges and opportunities inherent in the practical realization of quantum Otto engines [13]. The Single-Qubits of Quantum Otto engines operate on quantum working substances, typically two-level systems, harmonic oscillators, or many-body states, and their behavior under non-equilibrium conditions reveals complex phenomena influencing efficiency, work output, and power. This analysis delves into the detailed modeling of such engines within non-equilibrium environments, emphasizing the multifaceted influences of thermal gradients, external fields, noise, and decoherence

Recent developments in quantum thermodynamics have emphasized the pivotal role of measurement techniques and their influence on the performance of quantum Otto engines [14]. A series of impactful studies have elucidated how measurement strategies such as projective and weak measurements can be used not only for state readout but also as active tools to enhance energy transfer, work extraction, and efficiency [15].

The integration of quantum measurement protocols into Otto cycles, investigated by Son et al in Physical Review A, highlights that appropriately tailored measurement schemes induce coherence and correlations that elevate engine performance beyond classical limitations. Their findings suggest that measurement back-action can be harnessed as a resource in optimizing quantum thermodynamic processes [16]. Similarly, in PRX Quantum, he explores the interplay between measurement-induced disturbance and feedback control, demonstrating that measurement outcomes can be employed to implement feedback protocols that significantly improve work outputs and efficiency in quantum engines [17]. This work underscores the importance of measurement strategies as dynamic tools rather than passive observations. Earlier foundational studies, such as Physical Review E [18], investigate measurement-driven entropy production and the stochastic thermodynamics of quantum processes, emphasizing that the timing and strength of measurements critically influence irreversibility and efficiency. Additionally, Physical Review E [19] discusses the energetic costs associated with information gain through measurements, revealing that while measurements can boost performance, they also incur energetic overheads that must be carefully balanced [20]. These works collectively illustrate that measurement processes are integral to the control and optimization of quantum engines, especially in non-equilibrium regimes. They open pathways for utilizing measurement back-action and quantum feedback to push the boundaries of quantum thermodynamic efficiency and work extraction.

While idealized models of quantum Otto engines have provided foundational insights into quantum thermodynamics [1–6], they often fall short in capturing the complexities of real-world implementations. These idealized models, which typically assume perfect adiabaticity and negligible decoherence, predict efficiencies bounded by the Carnot limit. In contrast, our simulations explicitly consider non-equilibrium conditions like thermal gradients, external fields, and various decoherence channels, revealing efficiencies that can fall below the Carnot limit due to irreversible processes and energy dissipation. This highlights a critical divergence from idealized scenarios, underscoring the need to account for realistic environmental constraints in engine design [13].

Existing research has individually explored the impact of specific non-equilibrium effects, such as thermal gradients and decoherence [3],[7], on quantum engine performance. For example, studies on decoherence have primarily focused on Markovian processes [8], demonstrating their detrimental impact. Our work extends these investigations by not only considering the interplay between thermal gradients and multiple decoherence channels but also by incorporating non-Markovian noise models. This allows for a more accurate representation of the engine's interaction with its environment, capturing memory effects often neglected in simplified models, which can lead to more complex decoherence dynamics [11].

Finally, many studies propose control protocols, such as shortcuts to adiabaticity, to optimize quantum Otto engine performance [21]. Our contribution complements these efforts by providing a framework for evaluating the effectiveness of diverse control strategies within the context of non-equilibrium effects. In particular, we demonstrate that the optimal control strategy may vary based on specific non-equilibrium conditions and the relative importance of performance metrics like efficiency and power output. This suggests that a more adaptive approach to control is vital for ensuring robust engine operation in real-world settings, underscoring the novelty of our framework for quantitatively assessing control strategy performance under realistic environmental conditions [4].

METHOD

1 Theoretical Model of Efficiency of Single-Qubit Otto Cycle System

This section provides an in-depth overview of the single-qubit quantum Otto cycle and its associated power characteristics, establishing a basis for comparison with more complex multi-qubit systems [22]. It highlights that the maximum power output correlates directly with the temperature difference between the reservoirs and the energy level spacing, emphasizing key parameters for optimizing quantum engine performance [21]. The fundamental quantum Otto engine includes two thermal reservoirs, two work interaction steps, and a single qubit undergoing two adiabatic and two isochoric processes [23]. As illustrated in Figure 1, the cycle comprises six stages (a)–(f), assuming positive energy flow during heat absorption from the environment.

The cycle begins at step (a), where the qubit, characterized by an energy gap ω_h, absorbs heat Q_h from a hot bath at temperature T_h over an interaction time t_h. In step (b), the qubit is projected into a definite state, removing any correlations with the bath [24],[25]. Step (c) involves transferring work W_1 corresponding to a reduction of the energy gap from ω_h to ω_c while the qubit is decoupled from the environment. During (d), the qubit interacts with a cold reservoir at temperature T_c for a period t_c, releasing heat $-Q_c$ if de-excitation occurs. Step (e) involves a second measurement to disentangle the qubit, and at (f), the energy gap is elevated back to ω_h, facilitating a transfer of work W_2. Repetition continues until a steady limit cycle is established, verified through energy conservation: $\Delta E = |Q_h + Q_c + W_1 + W_2|$ where each term represents the respective energy exchanged during the cycle.

The adiabatic steps (c) and (f) correspond to compression and expansion, respectively, while steps (a) and (d) are isochoric processes that involve interactions between the system and baths modeled under a Non-Markovian framework. The dynamics of the single-qubit system in contact with these baths are typically examined via a master equation framework [26]. To quantify work output throughout the cycle, an indirect measurement protocol is employed, which tracks the energy exchanged with the work storage device without causing disturbance to the system's evolution, thereby optimizing the work extraction phase. Considering that interactions between qubits often influence the thermodynamic behavior in quantum systems. Such couplings have been shown to enhance efficiency and potentially boost power output, as previous research indicates the internal interactions significantly impact thermodynamic performance, including efficiency [27–29]. Exploring the power, efficiency, and work output of quantum Otto engines remains a promising area for future investigation.

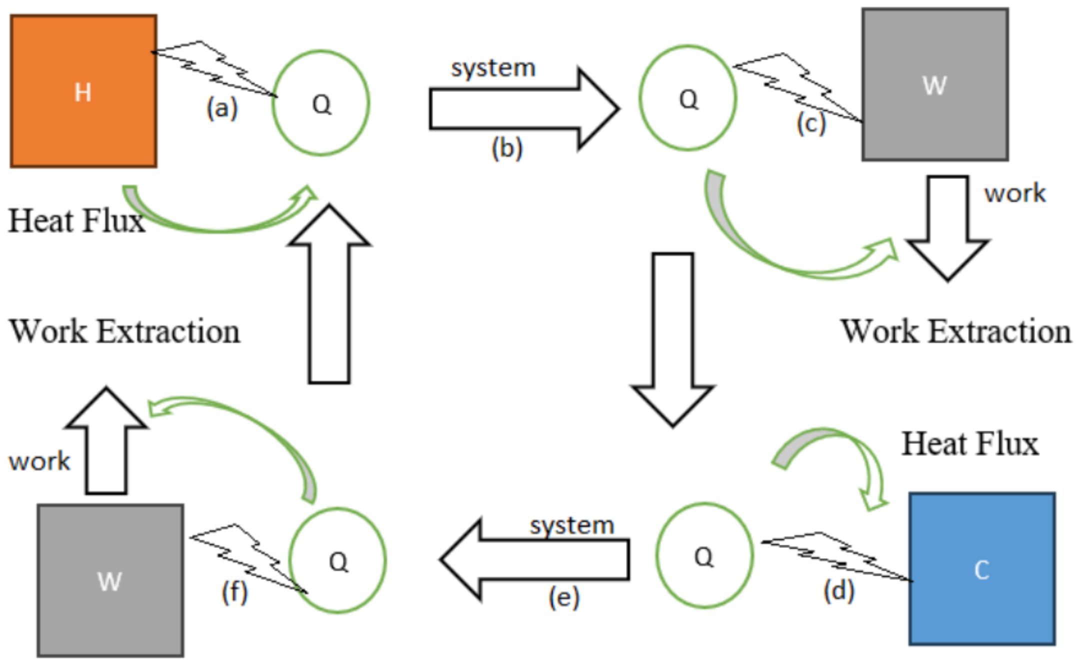

Figure 1. Schematic Diagram of Single Quantum Qubit

The theoretical model of the efficiency of a single-qubit Otto cycle system fundamentally revolves around the interplay between quantum energy levels, population distributions, and thermodynamic parameters. In this model, the working medium is typically represented as a two-level quantum system, where the energy eigenstates are modulated by external control parameters such as electric fields and dipole-dipole interactions. During the adiabatic strokes, these parameters are varied slowly enough to preserve the populations of the energy levels, ensuring a quantum adiabatic process. The thermalization steps at constant volume allow the system to exchange heat with hot and cold reservoirs, reaching equilibrium states characterized by Boltzmann distributions. The cycle's efficiency hinges on the difference in energy populations between the two equilibrium states and the energy gaps modulated by the external fields, which together determine the net work output.

Mathematically, the efficiency is expressed as the ratio of net work output to the heat absorbed from the hot reservoir. Considering the energy eigenvalues E_n^h and E_n^c during the hot and cold isochoric processes and the respective occupation probabilities p_n^h and p_n^c, the efficiency formula accounts for the energy differences weighted by population differences:

$$\eta = \frac{\sum_n \quad (E_n^h - E_n^c)(p_n^h - p_n^c)}{\sum_n \quad E_n^h p_n^h} \tag{1}$$

This relationship emphasizes that the efficiency is maximized when the energy levels are modulated to optimize the difference between populations subjected to thermalization at different temperatures, thereby maximizing work extraction. Effectively, the cycle converts thermal energy into mechanical work at the quantum level, and the efficiency is constrained by quantum and thermodynamic principles, including the second law.

Critically, the model underscores the importance of quantum coherence and adiabaticity in the cycle’s performance. Perfect adiabaticity ensures energy populations are preserved, minimizing dissipation, but in practical scenarios, non-adiabatic effects and quantum decoherence can reduce efficiency. Additionally, the model assumes idealized thermalization and control over system parameters, whereas real systems face challenges such as finite-time effects and environmental noise. These factors limit the achievable efficiency and highlight the need for optimized protocols that balance adiabaticity, cycle speed, and coherence preservation to approach the theoretical efficiency limits of single-qubit quantum Otto engines.

1.1 The Process of Work Extraction Using Quantum Measurement Theory

This subsection introduces a novel approach to quantum work extraction grounded in measurement-based quantum thermodynamics, emphasizing indirect measurement techniques. The proposed framework advances the understanding of energy transfer processes at the quantum level, highlighting both theoretical foundations and practical implications. Traditional thermodynamic descriptions of work at the quantum scale often rely on prospective measurements that can disturb system coherence. Our methodology employs an indirect measurement protocol where energy exchanges are inferred from the system’s Hamiltonian, offering a resolution of energy transfer events during work extraction [5]. The combined system encompasses the working qubit and a work reservoir, described by the Hamiltonian modeling. The Modeling of the Quantum Working Substance involves defining the quantum working substance (QWS), often modeled as a two-level system (TLS) with a Hamiltonian $H(t) = \frac{\hbar\omega(t)}{2}\sigma_z$, where $\omega(t)$ is the controllable energy gap. The cycle comprises four strokes: two adiabatic (or approximately adiabatic) processes where $\omega(t)$ varies, and two thermalization strokes where the system interacts with hot and cold reservoirs [30],[31].

Underlying the analysis are the dynamics governed by quantum master equations (QMEs), typically of Lindblad form, to incorporate dissipative effects

$$\frac{d\rho}{dt} = -\frac{i}{\hbar}[H(t), \rho] + D[\rho], \tag{2}$$

where $D[\rho]$ encapsulates environment-induced decoherence and dissipation mechanisms.

In non-equilibrium environments, reservoirs are characterized by non-thermal distributions, thermal gradients, and structured spectral densities, which significantly deviate from ideal thermal baths. These reservoirs sustain non-thermal steady states (NESS) in the system, altering the thermodynamic behavior and performance of quantum heat engines [32],[33]. To model this scenario, we used the system's evolution, which is described by generalized quantum master equations (GQMEs) that incorporate the effects of non-thermal spectral densities and distributions.
The dynamics of the system's density matrix $\rho(t)$ can be expressed as

$$\frac{d\rho}{dt} = -i[H_S, \rho] + D_{neq}[\rho] \tag{3}$$

where H_S is the system Hamiltonian, and D_{neq} is a non-equilibrium dissipator that accounts for structured spectral densities and non-thermal occupation functions. It typically takes the form:

$$D_{neq}[\rho] = \sum_{\omega} \quad J(\omega)\left[\left(N_{neq}(\omega) + 1\right)L[A(\omega)] + N_{neq}(\omega)L[A^{\dagger}(\omega)]\right] \tag{4}$$

where $J(\omega)$ is the spectral density describing the reservoir coupling strength at frequency $\omega, A(\omega)$ and $A^{\dagger}(\omega)$ are system operators corresponding to transitions at frequency $\omega, N_{neq}(\omega)$ is the non-thermal occupation number, which generalizes the distributions to $N_{neq}(\omega) \neq \frac{1}{e^{\frac{k_1\omega}{k_B T}} \mp 1}$ reflecting deviations such as nonthermal populations or energy-dependent biases. The steady state ρ_{NESS} of the system in such a non-equilibrium setting does not obey the detailed balance condition characteristic of thermal equilibrium, but instead satisfies $L[\rho_{NESS}] = 0$ where L is the Liouvillian superoperator derived from the GQME.

The modification of thermodynamic quantities early in the cycle involves redefining heat flows and entropy production. The heat exchanged with the reservoir during a process becomes:

$$Q_{neq} = \int_0^{\tau} \quad dt Tr\left[H_S \frac{d\rho}{dt}\right] \tag{5}$$

which now includes contributions from non-thermal distributions and structured spectral interactions.

The entropy production rate in such systems is expressed as

$$\dot{S}_{prod} = -\frac{d}{dt}S(\rho) + \sum_k \beta_k Q_k \quad (6)$$

where $S(\rho) = -\mathrm{Tr}[\rho \ln \rho]$ is the von Neumann entropy, and β_k are generalized inverse temperatures associated with each reservoir k, which may be frequency dependent or non-equilibrium in nature. Finally, the engine efficiency in these non-equilibrium settings must account for entropy production associated with the structured reservoirs is $\eta_{NE} = \frac{W_{cycle}}{Q_{input,NE}}$ where $Q_{\text{input, NE}}$ includes the effective heat provided by reservoirs with non-thermal features, and the total work W_{cycle} accounts for the energy exchange in the presence of sustained non-thermal conditions.

The impact on entropy and thermodynamic performance due to decoherence that leads to increased entropy, $S(\rho)$ $S(\rho) = -k_B \mathrm{Tr}[\rho \ln \rho]$, with the consequence that the system's pure state coherence diminishes over time, approaching a mixed state with classical correlations. $\rho(t) \rightarrow \rho_{\text{classical}}$ as $t \rightarrow \infty$ This process reduces the quantum advantage of enhanced work extraction and efficiency in quantum thermodynamic devices. This framework captures how structured spectral densities and non-thermal distributions modify the fundamental thermodynamic quantities and performance bounds of quantum Otto cycles in non-equilibrium environments.

1.2 Noise and Decoherence

Decoherence and noise are critical factors that limit the performance of quantum Otto engines in realistic environments. Understanding their specific effects is essential for designing strategies to mitigate their impact. Here, we delve into specific decoherence models and noise sources relevant to single-qubit quantum Otto engines.

1.2.1 Modeling Decoherence via Quantum Master Equations (QMEs)

The dynamics of a quantum system interacting with its environment (bath) can be described by a Lindblad Master Equation:

$$\frac{d\rho(t)}{dt} = -\frac{i}{\hbar}[H_S, \rho(t)] + D[\rho(t)] \quad (7)$$

where $\rho(t)$ is the system's density matrix, H_S is the system Hamiltonian, $D[\rho(t)]$ is the Lindblad dissipator capturing decoherence and dissipative effects. The dissipator for decoherence processes, such as phase damping or amplitude damping, typically takes the form

$$D[\rho] = \sum_k \quad \gamma_k \left(L_k \rho L_k^\dagger - \frac{1}{2}\{L_k^\dagger L_k, \rho\} \right) \tag{8}$$

where γ_k are the decoherence (or decay) rates, L_k are Lindblad operators modeling specific noise channels, which are dephasing and relaxation. Phase damping (dephasing) $L_k = \sigma_z$, with decoherence rate γ_ϕ The off-diagonal terms of ρ, which encode quantum coherence, decay as $\rho_{ij}(t) \sim e^{-\Gamma_\phi t}$ with $\Gamma_\phi = \gamma_\phi$

In Decoherence Models, we have amplitude damping which represents energy dissipation from the qubit to the environment, causing transitions from the excited state |1⟩ to the ground state |0⟩. This process is characterized by the amplitude damping rate (γ_1). The Lindblad operator for amplitude damping $L_1 = \sqrt{\gamma_1}\sigma^-$ where (σ^-) is the lowering operator. This amplitude is given by: $L_1 = \gamma_1\sigma$ damping reduces the population of the excited state, diminishing the engine's ability to extract work. It leads to a decrease in both efficiency and power output, as energy is lost to the environment. In the case of Phase damping, or dephasing, it disrupts the phase coherence between the qubit's states without energy loss. It is characterized by the dephasing rate ($\gamma\phi$). The Lindblad operator for phase damping is $L\phi = \sqrt{\gamma\phi}\sigma_z$ where (σ_z) is the Pauli-Z operator. Therefore, dephasing destroys quantum coherence, which is crucial for quantum enhancement in the engine cycle. It reduces the efficiency of the engine by suppressing quantum interference effects that could otherwise boost work extraction. In more complex scenarios, a combination of amplitude and phase damping may occur. A generalized model can be represented by $D[\rho] = \sum_i \gamma_i (L_i \rho L_i^\dagger - \frac{1}{2} L_i^\dagger L_i, \rho)$ where (γ_i) are the decoherence rates and (L_i) are the Lindblad operators for different decoherence channels. This interplay between different decoherence channels leads to complex dynamics, where mitigating one channel may exacerbate the effects of another.

1.2.2 Modeling Noise via Bath Spectral Density

To investigate the dynamics of a single-qubit quantum Otto engine and explore non-equilibrium effects based on the Lindblad master equation framework. The simulations were performed under the system-bath coupling and Non-Markovian dynamics [33–35].
During the cycle steps (a) and (d), the qubit interacts sequentially with the hot and cold thermal reservoirs, as depicted in Figure 1. The dynamics governing this open-system evolution are described by a Lindblad master equation:

$$\frac{d\rho}{dt} = -i[H_S^\alpha, \rho] + L_\alpha \rho \tag{9}$$

Here, the Lindblad superoperator L_α captures the dissipative effects of the baths under a weak-coupling approximation:

$$L_\alpha\rho = \Gamma_\alpha(-\omega_\alpha)\left(\sigma^-\rho\sigma^+ - \frac{1}{2}\{\sigma^+\sigma^-,\rho\}\right) + \Gamma_\alpha(\omega_\alpha)\left(\sigma^+\rho\sigma^- - \frac{1}{2}\{\sigma^-\sigma^+,\rho\}\right)(10)$$

where $\sigma^+$and $\sigma^-$are the raising and lowering operators, respectively. The rates $\Gamma_\alpha(\pm\omega)$ depend on the bath spectral density and thermal occupation $\Gamma_\alpha(\omega) = G_\alpha(\omega) = \gamma_\alpha(\omega)[1 + n^-{}_\alpha(\omega)]$, for $\omega > 0$ and $G_\alpha(-\omega) = \gamma_\alpha(\omega)n^-{}_\alpha(\omega)$ with the average occupation $n^-{}_\alpha(\omega) = \frac{1}{e^{\omega/(k_B T_\alpha)}-1}$

The spectral density $\gamma_\alpha(\omega)$ captures the bath modes and is modeled as an Ohmic spectrum:

$$\gamma_\alpha(\omega) = 2\pi \sum_\mu g^2_{\mu,\alpha}\delta(\omega - \omega_{\mu,\alpha}) \equiv 2\pi J_\alpha(\omega) \tag{11}$$

for positive frequencies, with $J_\alpha(\omega)$ typically chosen as:

$$J_\alpha(\omega) = \kappa_\alpha \frac{\omega^s}{\omega_{c,t}^{s-1}} exp\left(-\frac{\omega}{\omega_{c,t}}\right) \tag{12}$$

where $\omega_{c,t}$ denotes a cutoff frequency, κ_α represents the coupling strength, and $s = 1$ characterizes an Ohmic environment. Environmental noise can be characterized by a spectral density $J(\omega)$, which determines how the environment couples to the system modes:

$$J(\omega) = \sum_j |g_j|^2 \delta(\omega - \omega_j) \tag{13}$$

In the continuum limit, commonly used spectral densities include: Ohmic: $J(\omega) = \eta\omega e^{-\omega/\omega_c}$, Super-Ohmic or sub-Ohmic depending on the physical environment. This spectral density influences decoherence rates and thermalization times, $\Gamma(\omega) \sim J(\omega)[1 + n(\omega)]$ where $n(\omega)$ the occupation number is a frequency ω. Noise sources we have thermal noise, which arises from the random thermal fluctuations in the environment, causing the qubit to interact with a thermal bath.

Thermal noise introduces random transitions between the qubit's energy levels, disrupting the adiabatic processes in the Otto cycle. This reduces the engine's efficiency and stability, especially at higher temperatures. Cooling the environment to reduce thermal fluctuations can mitigate thermal noise. Additionally, implementing error correction techniques may help to counteract the effects of thermal noise. In electromagnetic noise, which includes fluctuations in electric and magnetic fields that interact with the qubit. These fluctuations induce unwanted transitions and disrupt the qubit's energy levels. Electromagnetic noise causes significant decoherence and energy loss, reducing the engine's efficiency and work output. Shielding the qubit from external electromagnetic radiation and using materials with low dielectric loss can reduce electromagnetic noise. Dynamical decoupling techniques are also be employed to suppress the effects of electromagnetic noise. Parameter fluctuations which refers to the variations in the control parameters of the engine, such as energy level spacings or coupling strengths, due to imperfections in the control apparatus. These fluctuations disrupt the precise timing and execution of the Otto cycle, leading to deviations from the ideal adiabatic and isochoric processes. Implementing feedback control mechanisms to stabilize the control parameters and using robust control techniques that are less sensitive to parameter variations can mitigate the effects of parameter fluctuations. Non-Markovian noise in Real-world environments often exhibits memory effects, meaning that the noise at a given time depends on the system's past. This is described as non-Markovian noise whose impact on engine performance leads to more complex decoherence dynamics, including revivals of coherence at certain times in Modeling we Captured via bath correlation functions ($C(t)$), reflecting the environment's memory. The system's dynamics are then described by integro-differential equations, accounting for the non-local-in-time effects.

1.3 Dynamics of the Non-Markovian Environment Qubit Models in Non-Equilibrium Conditions

In open quantum systems, the dynamics of a system coupled to an environment (or bath) are significantly influenced by the properties of that environment. When the environment exhibits memory effects—meaning its future evolution depends on past interactions—the dynamics are termed non-Markovian. This situation contrasts with Markovian models, where memory effects are negligible, and the evolution is effectively memoryless. The efficiency and performance of quantum heat engines, such as the Quantum Otto cycle implemented with a single qubit, strongly depend on the nature of the system-environment interactions. When the environment exhibits non-Markovian, memory-dependent effects, the dynamics deviate from simple Markovian decay, leading to possible recoherence, information backflow, and altered thermodynamic behavior. In non-equilibrium environments, the bath may not be in thermal equilibrium, initially prepared in a non-thermal state, or subject to external driving, further complicating the system's dynamics. Modeling these effects accurately involves understanding how environmental noise characterized through the bath spectral density ($J(\omega)$) influences the qubit during the thermodynamic cycle.The environmental influence on the system has been encapsulated via a spectral density function $J(\omega)$, which characterizes how different bath modes couple to the system and their respective frequencies. This spectral density describes the distribution of environmental modes and their coupling strengths and fundamentally determines the nature of the system-environment interaction, especially its temporal correlations.The total Hamiltonian encompasses the system (single qubit), the environment (bath), and their interaction

$$H_{total} = H_S(t) + H_B + H_{SB} \tag{14}$$

System Hamiltonian of the single qubit with a time-dependent energy splitting $H_S(t) = \frac{\hbar\omega(t)}{2}\sigma_z$, where (σ_z) is the Pauli-Z operator and $(\omega(t))$ the controllable frequency for the Otto cycle. The bath Hamiltonian $H_B = \sum_k \quad \hbar\omega_k b_k^\dagger b_k$. Interaction Hamiltonian assuming a linear coupling between the qubit and the bath modes $H_{SB} = \sigma_x \sum_k \quad g_k(b_k + b_k^\dagger$ or, alternatively, $H_{SB} = \sigma_z \sum_k \quad g_k\left(b_k + b_k^\dagger\right)$ depending on the coupling mechanism.

The spectral density function is defined as the bath's influence is encapsulated via its spectral density

$$J(\omega) = \sum_k \quad |g_k|^2 \delta(\omega - \omega_k) \tag{15}$$

In the continuum limit, common spectral forms include: $J(\omega) = \eta\omega^s e^{-\omega/\omega_c}$ where (η) is the coupling strength, (s) determines whether the environment is sub-Ohmic, Ohmic, or super-Ohmic, and (ω_c) is the cutoff frequency. Unlike Markovian models, which assume a memoryless bath leading to exponential decay, non-Markovian environments exhibit memory effects captured via bath correlation functions $C(t) = \langle B(t)B(0)\rangle_B$ where $\left(B(t) = \sum_k g_k\left(b_k e^{-i\omega_k t} + b_k^\dagger e^{i\omega_k t}\right)\right)$. Bath correlation function expressed via the spectral density

$$C(t) = \int_0^\infty \quad d\omega, J(\omega)\left[coth\left(\frac{\hbar\omega}{2k_BT}\right)cos(\omega t) - isin(\omega t)\right] \tag{16}$$

In non-equilibrium conditions, the bath state $\left(\rho_B^{non-eq}\right)$ may not be thermal. This modifies $(C(t))$, which then includes contributions from non-thermal distributions or external disturbances, leading to $C_{non-eq}(t) \neq C_{thermal}(t)$ the environment exhibits time-dependent, non-stationary noise. In non-equilibrium environments, the bath was driven, initially prepared in a non-thermal state, and time-dependent. The influence on system evolution is then described by a non-local-in-time reduced dynamics, often formulated using the Feynman-Vernon influence functional or path integral methods, capturing the system's memory effects

1.3.1 Formal Description of Non-Markovian Effects using Quantum Master Equation

The reduced density matrix $\rho_S(t)$ of the system evolves according to a generalized master equation:

$$\frac{d}{dt}\rho_S(t) = -\frac{i}{\hbar}[H_S, \rho_S(t)] + K(t, t_0)[\rho_S(t)] \tag{17}$$

where the memory kernel $K(t, t_0)$ encodes the non-Markovian effects, often expressed as an integro-differential equation:

$$\frac{d}{dt}\rho_S(t) = -\frac{i}{\hbar}[H_S, \rho_S(t)] - \int_{t_0}^{t} ds\Sigma(t-s)\rho_S(s) \tag{18}$$

with $\Sigma(t-s)$, the bath correlation function, related to the spectral density:

$$C(t) = \langle B(t)B(0)\rangle_B = \int_0^{\infty} d\omega J(\omega)\left[coth\left(\frac{\hbar\omega}{2k_BT}\right)cos(\omega t) - isin(\omega t)\right] \tag{19}$$

under equilibrium conditions. For non-equilibrium baths, $C(t)$ is modified according to the initial bath state or driving protocols. Derivation of the Memory Kernel for a qubit coupled via (σ_z), and under the weak-coupling approximation (Born approximation), the Nakajima-Zwanzig projection operator technique yields $K(t-s) \propto C(t-s), \sigma_z \cdot \sigma_z$ Explicitly, the dynamical evolution involves correlation functions of environmental noise, leading to decoherence and relaxation processes that depend on the environment's memory. In the case of a general bath spectral density ($J(\omega)$), the time-dependent relaxation and dephasing rates can be characterized by $\Gamma(t) \sim \int_0^t ds, C(s)$ where the non-Markovian behavior manifests as non-exponential decay, with possible revivals or coherence recoherence at certain times due to information backflow.

In non-equilibrium conditions, the bath is not necessarily in thermal equilibrium, which influences the bath correlation functions and the resulting system dynamics. This can occur due to external driving, initial non-thermal states, or time-dependent bath parameters. The bath correlation function $C(t)$ then becomes $C(t) = \langle B(t)B(0)\rangle_B^{non-eq} = Tr_B\left[\rho_B^{non-eq} B(t)B(0)\right]$ where ρ_B^{non-eq} is the non-equilibrium bath density matrix. This deviates from the equilibrium form and can result in time-dependent spectral features, non-Lorentzian noise spectra, and altered decay behaviors. Bath Correlation Function (general non-equilibrium form)

$$C(t) = \int_0^{\infty} d\omega J(\omega)\left[coth\left(\frac{\hbar\omega}{2k_BT(\omega,t)}\right)cos(\omega t) - isin(\omega t)\right] \tag{20}$$

where $T(\omega, t)$ reflects non-equilibrium temperature-like parameters possibly varying with frequency and time. Generalized Master Equation with Memory Kernel:

$$\frac{d}{dt}\rho_S(t) = -\frac{i}{\hbar}[H_S, \rho_S(t)] - \int_{t_0}^{t} ds\Sigma(t-s)\rho_S(s) \tag{21}$$

where $\Sigma(t-s)$ is derived from the environment's spectral density and initial conditions. Modeling non-Markovian effects under non-equilibrium conditions involves understanding the bath spectral density $J(\omega)$, the resulting bath correlation functions $C(t)$, and their impact on the system's memory and dynamics. Such models are crucial for understanding complex quantum phenomena such as decoherence, information back-flow, and energy transfer in driven or nonthermal environments.

Results and Discussion

1 Environmental Factors on Quantum Otto Cycle

Environmental factors shape the performance and efficiency of quantum thermal machines operating within the framework of the Quantum Otto Cycle. An in-depth understanding of these external influences translates theoretical models into practical functioning devices. This section examines the interactions of temperature fluctuations, decoherence phenomena, and electromagnetic noise that impact the operation of the quantum cycle at the microscopic level.

External influences modify the thermodynamic properties of the working medium, affecting energy exchange processes and the stability of the cycle. Variations in ambient temperature can lead to thermal gradients that influence the populations of quantum states, thereby altering work output and efficiency. Decoherence effects, arising from coupling to surrounding environments, diminish quantum coherences and entanglement, reducing the potential quantum advantage in thermodynamic cycles.

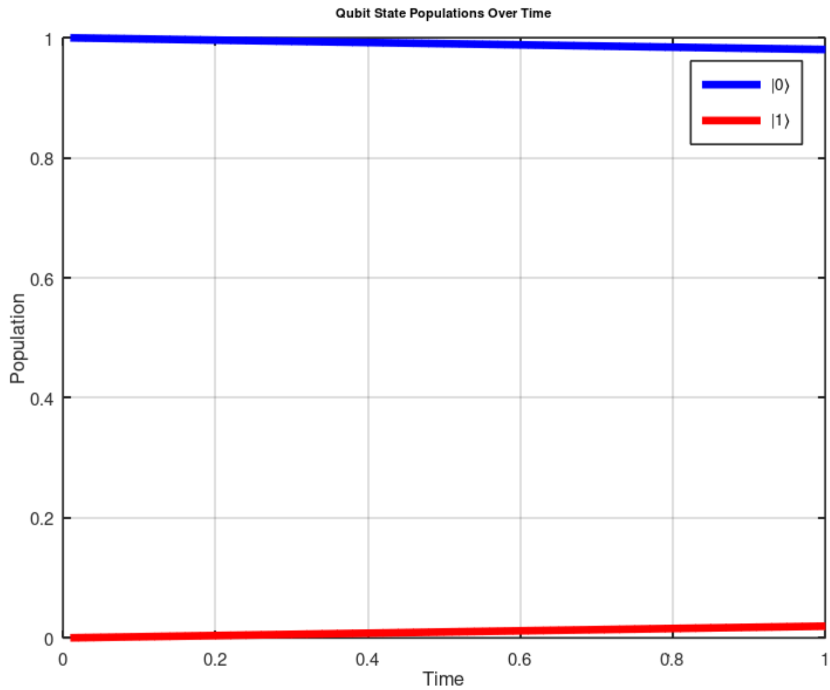
Qubit State Populations Over Time
Population
Time
|0⟩
|1⟩
0
0.2
0.4
0.6
0.8
1

(a)

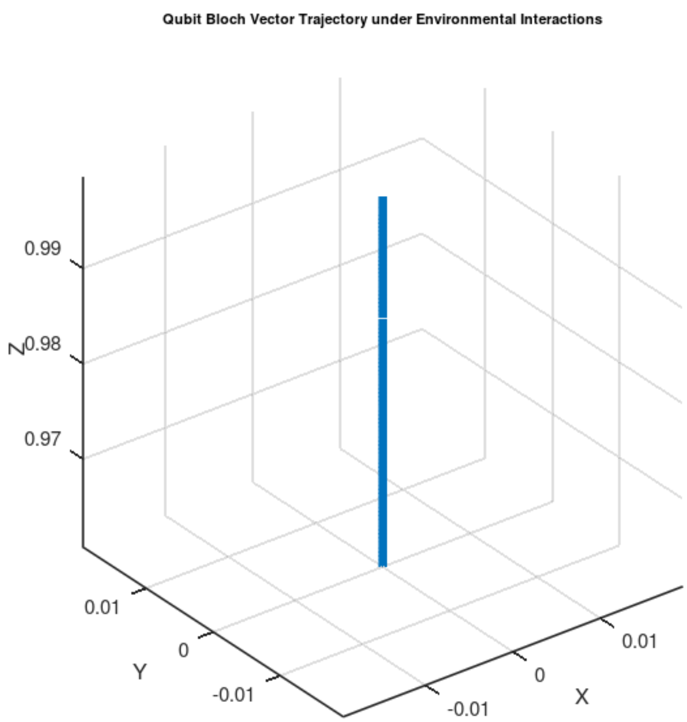
Qubit Bloch Vector Trajectory under Environmental Interactions
Z
0.99
0.98
0.97
Y
0.01
0
-0.01
X
0.01
0
-0.01

(b)

Figure 2. (a) This graph illustrates the time evolution of qubit state populations under the influence of environmental factors like temperature, electromagnetic noise, and decoherence. It employs a density matrix approach with Lindblad operators to visualize how the probabilities of the qubit being in state —0⟩ (blue line) and state —1⟩ (red line) change over time. (b)This plot depicts the trajectory of the qubit's Bloch vector on the Bloch sphere. The dynamics are modeled using a density matrix approach with Lindblad operators, which account for dephasing and bit-flip errors due to the environment.

Models a qubit interacting with an environment where temperature, electromagnetic noise, and decoherence phenomena influence its evolution. It employs a density matrix approach with Lindblad operators and visualizes the qubit's trajectory and state populations over time, as shown in Figure 2(a). The temperature fluctuates randomly within a specified amplitude, influencing the thermal population but not directly modeled in the current decoherence dynamics. This can be expanded upon. Quantum noise sources, both dephasing and bit-flip errors, are included via Lindblad operators, representing common environmental noise factors. Trajectory visualization by Bloch sphere plot, as illustrated in Figure 2(b) how the quantum state evolves under these effects over time. Electromagnetic noise contributes to fluctuations in the system's energy levels, contributing to dissipation and reducing cycle stability. Understanding these interactions provides vital insights for optimizing quantum heat engines, allowing for mitigation strategies such as environmental isolation, dynamical decoupling, or reservoir engineering. Consequently, this knowledge bridges the gap between idealized quantum thermodynamic models and real-world implementations, ensuring device robustness under practical operating conditions. In addition to thermal fluctuations, controlled manipulation of thermal gradients and the use of nonthermal reservoirs offer avenues to enhance the cycle's performance. External fields—particularly magnetic (**B**) and electric (**E**) serve as powerful tools to engineer the energy landscape of quantum systems, notably quantum well states (QWS).

1.1 M odification of Quantum Well States via External Fields

Applying magnetic or electric fields to a quantum well modifies its potential profile and boundary conditions, directly impacting the energy spectrum of confined electrons. These modifications enable precise control over energy gaps, facilitating adiabatic processes and influencing the thermodynamic pathways of the cycle. Furthermore, external fields can induce quantum coherence and entanglement within the working medium, potentially enabling quantum advantages such as enhanced work extraction or efficiency surpassing classical bounds. The ability to tune the system's energy spectrum through external fields introduces a versatile mechanism to optimize cycle parameters dynamically. This control over quantum states not only modifies thermodynamic properties but also provides a pathway for utilizing quantum correlations as resources, further influencing heat and work exchanges.

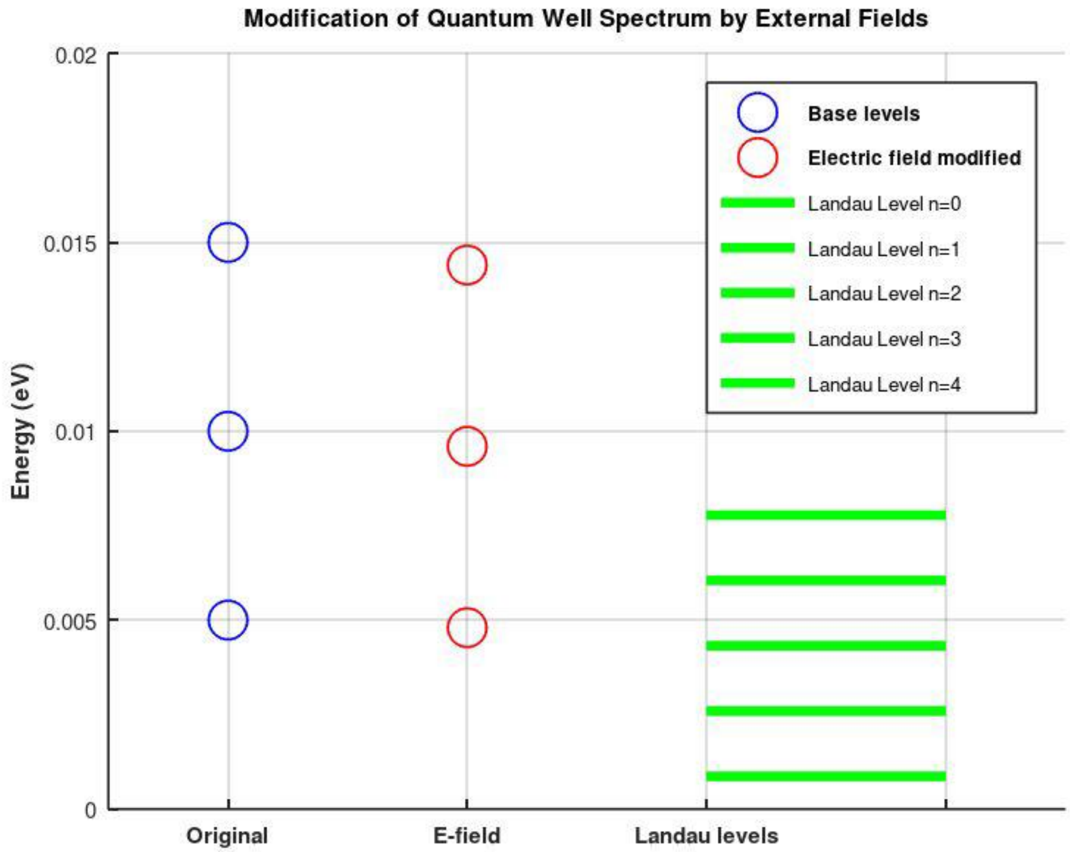

Figure 3: Illustrates how the energy levels are modified by external fields and provides a framework to analyze their impact on quantum thermodynamics in a quantum Otto engine context for parameters $m^* = 0.067 * 9.11^{-31}$; effective mass of electron in kg, $\hbar = 1.055^{-34}$, reduced Planck constant, $(Js) e = 1.602^{-19}$; elementary charge (C). The Quantum well parameters $E_{n_{base}} = [5^{-3}, 10^{-3}, 15^{-3}]$: Base energy levels in eV for ($n = 1,2,3$) Convert eV to Joules $E_{n_{base}} = E_{n_{base}} * e$; and the external fields parameters $E_{field} = 1^5$, electric field in V/m, $B_{field} = 1.0$. Magnetic field in Tesla

The model shows the effects of electric and magnetic fields on the energy spectrum of electrons in a quantum well, considering both Stark shifts and Landau quantization. The energy spectrum without external fields can be described by the basic Hamiltonian for electrons in a quantum well along the z-direction (confined potential $V(z)$) is $H_0 = \frac{p_z^2}{2m^*} + V(z)$ where m^* is the effective mass. The solutions give quantized energy levels $E_n^{(0)}$ with corresponding wavefunctions $\psi_n^{(0)}(z)$. The effect of electric fields that are uniform E, applied along the confinement direction (say, z-axis), introduces an additional potential $V_E(z) = eEz$, This can be a modified Hamiltonian, which becomes $H_E = H_0 + eEz$. This field tilts the potential, inducing a Stark shift in energy levels as $\Delta E_n \approx -eE\langle z \rangle_n$ where $\langle z \rangle_n$ is the expectation value of position for state n, and the energy levels shift as $E_n(E) = E_n^{(0)} + \delta E_n$ with $\delta E_n \propto E$. This allows control of the energy gap $\Delta E_{mn} = E_m - E_n$. The effect of a magnetic field B (for simplicity, along the z-axis) introduces both orbital and spin effects. The orbital effect modifies the momentum via minimal coupling of $p \rightarrow p +$

eA, where A is the vector potential, e.g., in Landau gauge $A = (-By, 0,0)$. Therefore, the kinetic Hamiltonian becomes $H_B = \frac{1}{2m^*}(p + eA)^2$. This leads to Landau quantization for free electrons in 2D $E_{n,k_z} = \hbar\omega_c\left(n + \frac{1}{2}\right) + \frac{\hbar^2 k_z^2}{2m^*}$. where $\omega_c = \frac{eB}{m^*}$this quantizes the in-plane energy spectrum, creating Landau levels. By tuning E and B, the system can be driven into regimes where quantum coherence C and entanglement E are enhanced $C(t) \sim |\langle\psi_1(t) \mid \psi_2(t)\rangle|$, $E \sim$ as a function of off-diagonal density matrix elements. Control over E and B affects the evolution of the system's state, potentially enabling quantum advantages in thermodynamic processes, such as work extraction or heat flow

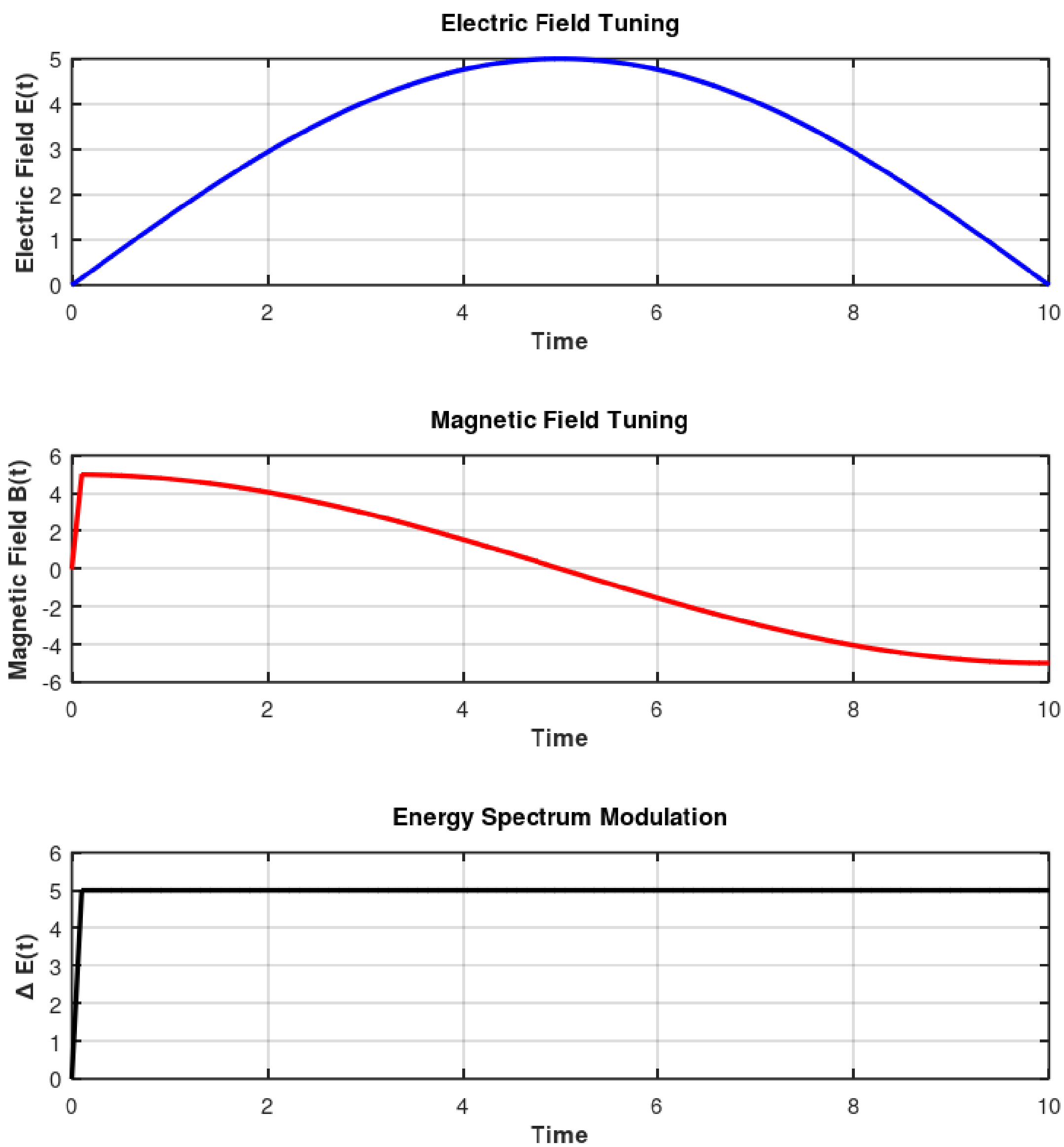

Figure 4 shows how the energy levels of a quantum well are modified by external fields with these parameters: $m *= 0.067 * 9.11 - 31$, effective mass of electron in kg, $\hbar = 1.055^{-34}$, Reduced Planck constant, $(Js)e = 1.602^{-19}$, and elementary charge (C). The Quantum well parameters $E_{nbase} = [5^{-}3, 10^{-}3, 15^{-}3]$; Base energy levels in eV for $(n = 1,2,3)$ Convert eV to Joules $E_{n\,base} = E_{n\,base} * e$; and the external fields parameters $E_{field} = 15$; electric field in $V/m, B_{field} = 1.0$ Magnetic field in Tesla. The graph illustrates how electric and magnetic field tuning can control quantum coherence and entanglement

Modifying the energy spectrum influences the thermodynamic properties, including the energy gap $\Delta E(t)$, which plays a crucial role in adiabatic and non-adiabatic transitions $\frac{dE(t)}{dt}$ can be controlled to manage adiabaticity Quantum coherence and entanglement contribute to thermodynamic advantages, for instance, through enhanced work extraction via quantum stimulative effects.

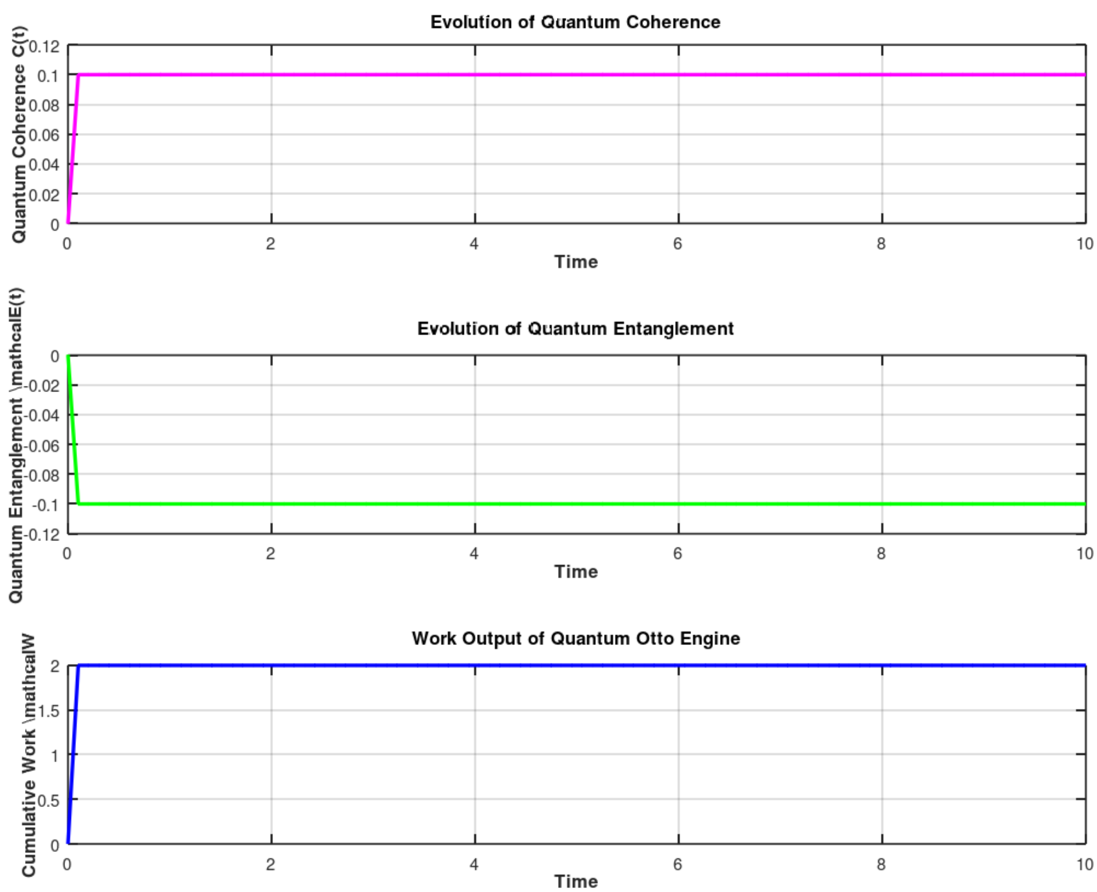

Figure 5 illustrates the dynamics of quantum coherence, entanglement, and work output in a Quantum Otto Engine system. It visualizes the interplay between these quantum properties and thermodynamic performance

External magnetic and electric fields provide tunable parameters to engineer the energy spectrum of QWS, influence coherence and entanglement, and enable quantum control in thermodynamic coherent state $|\psi\rangle$, driven by a protocol optimized for quantum coherence, experiences decoherence characterized by a coherence mmeasure $C(t)$ $C(t) = |\langle\psi(t)|\rho(t)|\psi(t)\rangle| \sim e^{-\Gamma t}$. The maximum achievable work $W_{\max}$ in a quantum process can be expressed as

$W_{\max}(t) \approx W_{\text{quantum, initial}} \times C(t)$ indicates that decoherence diminishes the quantum advantage proportionally to the decay of coherence. Environmental noise modeled through Lindblad equations, bath spectral densities, and decoherence rates causes decoherence and entropy increase, thereby reducing the quantum advantages in thermodynamic systems and limiting their performance.

1.2 Power Output and Its Dependence on System Dynamics in Non-Equilibrium

The instantaneous power $P(t)$ relates to the rate of energy change in the system $P(t) = -\langle\frac{\partial H_S(t)}{\partial t}\rangle$ which accounts for the explicit time dependence of $H_S(t)$. The average power over a cycle or operation is $\langle P\rangle = \frac{1}{T}\int_0^T P(t)dt$ Where appropriate, the heat flux between the system and environment is derived from the reduced density matrix $\rho(t)\dot{Q}(t) = Tr\left[H_B \frac{d\rho_B(t)}{dt}\right]$, which influences power output indirectly through the system's non-equilibrium states. Power and Operational Regimes advances models reveal that time-dependent coupling can enhance power output by enabling synthetic control over energy transfer processes. Non-Markovian environments can lead to coherent effects that temporarily boost efficiency.

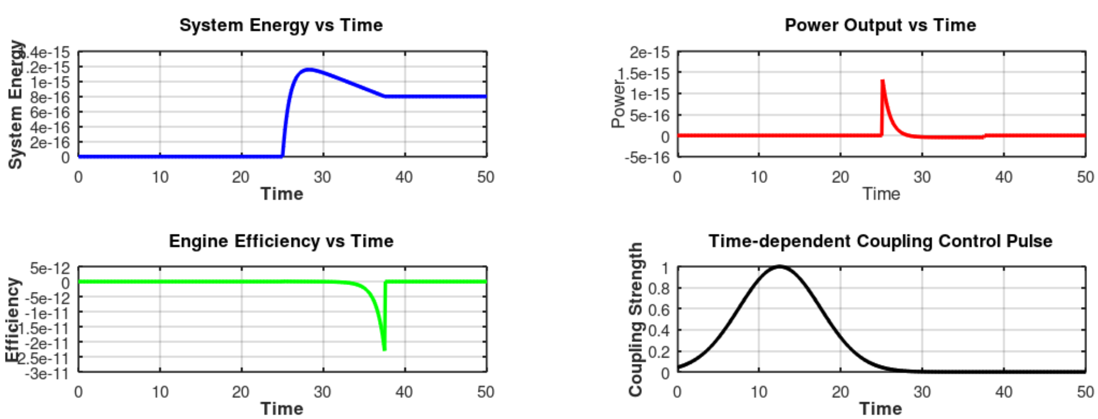

Figure 6. illustrates the relationships between system energy, engine efficiency, power output, and the time-dependent coupling control pulse into nonequilibrium operating regimes

The modification of operational regimes arises from these non-equilibrium effects, often captured by the interplay between system parameters, bath memory, and driving protocols. This framework provides an approach to modeling and understanding the behavior of far-from-equilibrium quantum systems, especially regarding their energy and power characteristics under complex driving and environmental influence. The performance and functioning of a quantum Otto cycle implemented, for instance, with a single qubit, are inherently sensitive to the surrounding environment. Several environmental factors can significantly alter energy exchanges, coherence properties, and the thermodynamic efficiency of the cycle. Environmental noise causes the qubit's coherent superpositions to decay (decoherence), and excited states to relax, which diminishes the ability to perform coherent work extraction. Environments with memory effects (non-Markovian) can temporarily transfer information back to the system, leading to non-trivial energy and coherence dynamics. Can prolong coherence times during the adiabatic strokes. Possible partial recovery of energy or coherence, leading to increased work output or efficiency. Coupling Strength between System and Environment Weak vs. Strong Coupling Weak coupling leads to Markovian, often exponential, decoherence and thermalization. Strong coupling introduces significant non-Markovian effects, coherences, and potentially nonuniform thermalization rates.

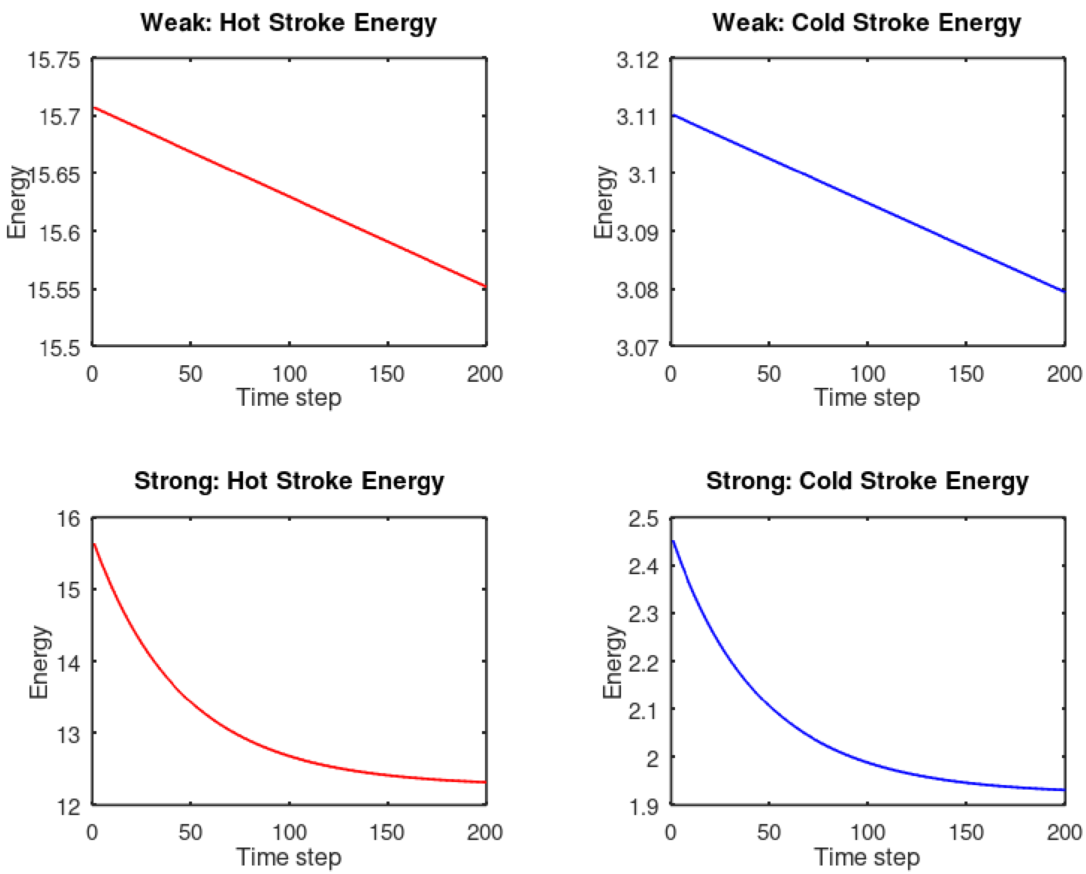

Figure 7. compares energy evolution during the hot (heat addition) and cold (heat rejection) strokes of a thermodynamic cycle under different system environment coupling strengths. The top row illustrates the energy change during the hot and cold strokes for weak coupling, typically associated with more Markovian dynamics. The bottom row shows the energy evolution for strong coupling, where non-Markovian effects and memory in the environment become significant. Comparing these plots highlights how the strength of the coupling affects the rate and nature of energy exchange between the system and its thermal reservoirs. This comparison illustrates different ways to optimize performance

Strong coupling environments cause deviations from standard thermodynamic behavior. Dynamic control of coupling strength is used to optimize performance.

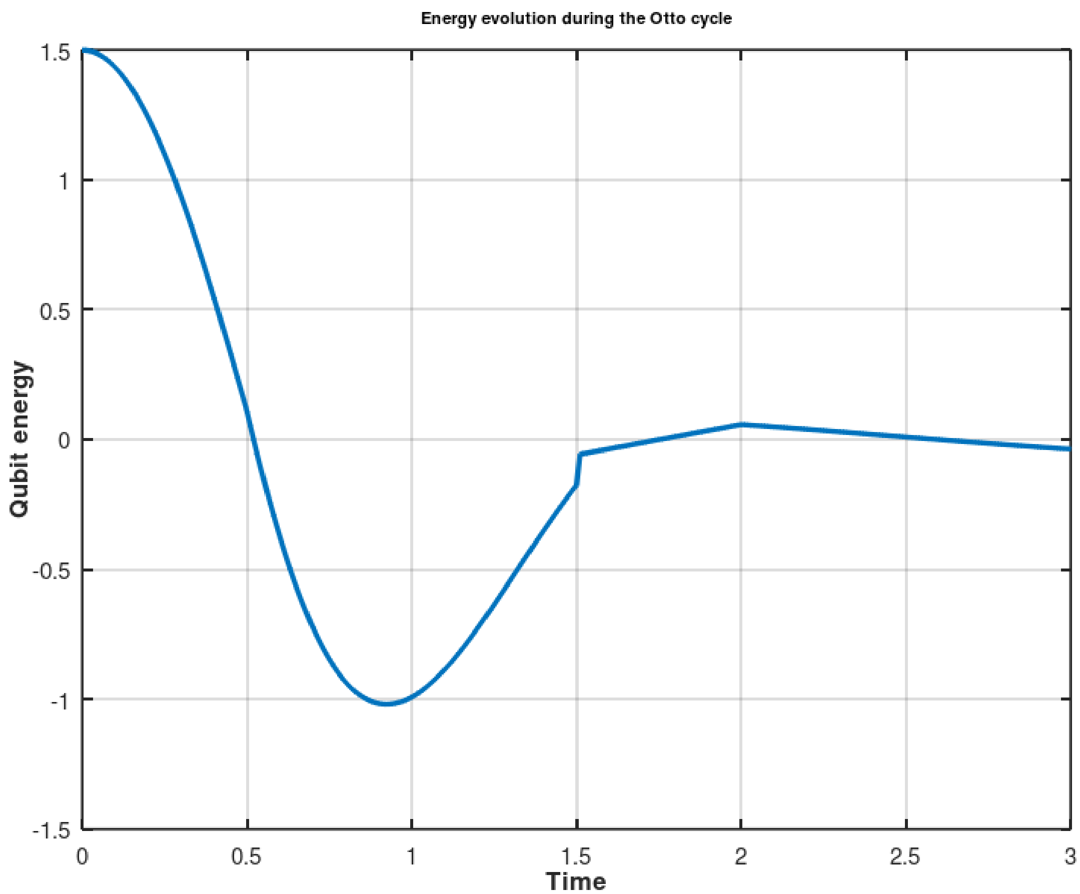

Figure 8. depicts the energy changes of a single-qubit working substance throughout the complete Quantum Otto cycle. The vertical axis represents the qubit energy, while the horizontal axis represents time, spanning the various stages of the cycle (adiabatic compression, hot isochore, adiabatic expansion, and cold isochore). Each segment of the plot corresponds to a specific process, showing how energy is added or extracted from the system at different stages

The engine's efficiency η is traditionally bounded by the Carnot limit, but in non-equilibrium contexts, this bound can be surpassed or reinterpreted depending on the nature of the reservoirs and the initial states. The work W per cycle is obtained from the difference in average energy during executive strokes $W = \mathrm{Tr}[H_1(\rho_2 - \rho_1)] + \mathrm{Tr}[H_3(\rho_4 - \rho_3)]$, where ρ_i are system states at different points. Power P considers the cycle duration, which is sensitive to external influences such as noise, which can slow down processes or introduce fluctuations.

In non-equilibrium environments, extra care was taken to partition the energy flows, accounting for entropy production and irreversibility introduced by the environment. Efficiency definitions may extend to considering non-thermal energy exchanges, leading to concepts of effective temperatures or generalized efficiencies. We numerically concentrate on the scenario in which the engine is the quantum Otto engine, using an idea that gives the structure of the full phase diagram, since we use power, efficiency, and the two performance coefficients. In a single-qubit Otto engine operating under non-equilibrium conditions, the heat coefficient of performance (HCOP) and the cooling coefficient of performance (CCOP) are critically linked through the engine's thermodynamic cycle parameters and quantum state dynamics. HCOP quantifies the engine's efficiency in converting heat absorbed from the hot reservoir into work, whereas CCOP measures its effectiveness in transferring heat away from the cold reservoir during the cooling process. Under non-equilibrium conditions, these performance metrics are interconnected because the same quantum interactions and energy exchanges that govern heat absorption and work output influence the engine's ability. Specifically, the parameters that maximize HCOP often impose constraints on CCOP, and vice versa, reflecting the fundamental trade-offs in quantum thermodynamic operations. This relationship highlights the delicate balance between energy transfer, coherence, and quantum state populations that underpin the engine's dual roles, emphasizing that improved performance in one mode typically affects the other, especially when driven away from thermal equilibrium.

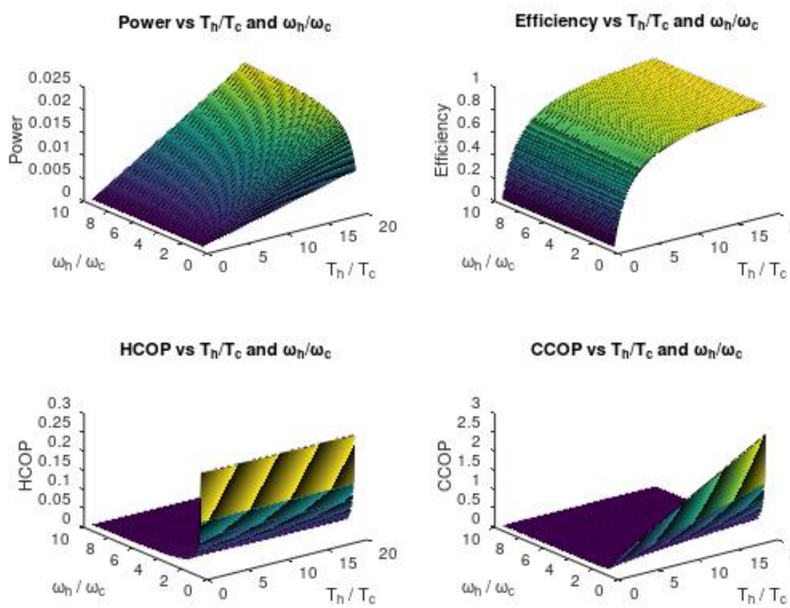

Figure 9. depicts the dependence of key performance metrics—power output, thermodynamic efficiency, Heat Coefficient of Performance (HCOP), and Cooling Coefficient of Performance (CCOP)—for a single-qubit Otto cycle under equilibrium conditions. It analyzes how these metrics vary as a function of two key ratios: the temperature ratio of the hot to cold reservoirs (T_h/T_c) and the ratio of the energy level spacings (ω_h/ω_c). The energy scale is normalized such that $\omega_c = 1$. The temperature of the cold environment is maintained at $T = 5$, with the transition coupling strengths for both hot and cold baths equal ($\kappa_h = \kappa_c = 0.005$). The interaction times are equal ($t_h = t_c = 50$*units*). The data deviates from this ideal behavior

In an idealized equilibrium setting, we expect the efficiency to increase steadily with both the temperature ratio and the energy level ratio, theoretically approaching the Carnot limit as T_h/T_c becomes very large [5,36,37]. Similarly, the power output should grow monotonically with these parameters, likely demonstrating a linear relationship with the energy level difference, reflecting a proportional increase in work extraction. The coefficients of performance for heat transfer, HCOP and CCOP, are anticipated to follow the behavior predicted by reversible thermodynamics, resembling a Carnot cycle.

However, the actual data depicted in Figure 9 reveal deviations from this ideal behavior, such as peaks in efficiency and non-monotonic dependence, which are indicative of non-equilibrium effects and irreversibility in the real system [38]. These discrepancies highlight the influence of finite-time effects, dissipative losses, and other non-idealities that diverge from the idealized thermodynamic limits.

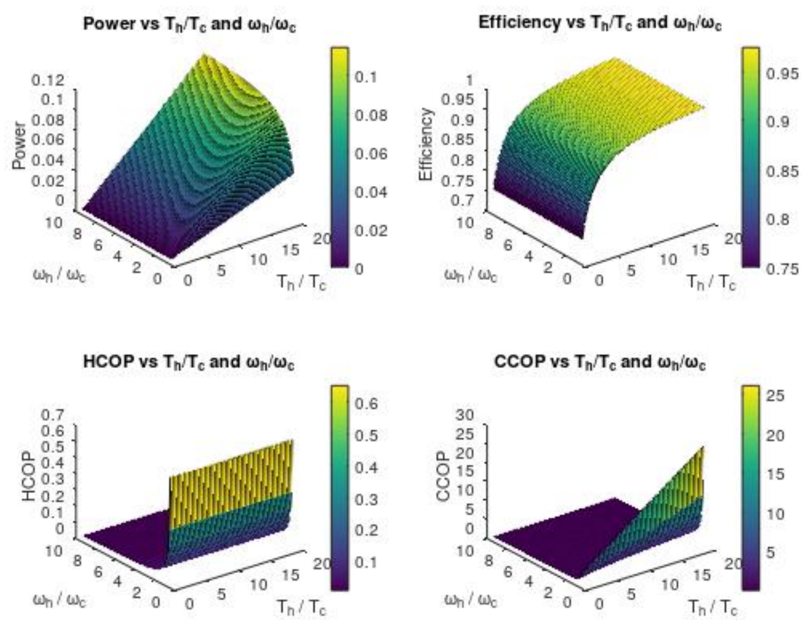

Figure 10. displays the behavior of power output, efficiency, heat coefficient of performance (HCOP), and cooling coefficient of performance (CCOP) for a single-qubit Otto engine functioning under non-equilibrium conditions. The parameters used include temperature ratios (T_h/T_c) and ratios of the energy level spacings (ω_h/ω_c). The 3D surface plots show that power increases with increasing both T_h/T_c and ω_h/ω_c but although efficiency generally increases, there is a clear optimum for each. Increasing excessively reduces efficiency

In Figure 10 the evaluation spans a spectrum of heat bath temperature ratios T_h/T_c and ratios of the energy level spacings ω_h/ω_c.. These results illustrate how each performance metric responds to varying thermodynamic parameters in a system operating away from equilibrium. This is intuitive because a larger temperature difference provides a greater driving force for the engine, and a larger energy level difference (ω_h/ω_c) means more work can be extracted per cycle. The relationship appears approximately linear with respect to both ratios within the plotted ranges [25,39]. The non-equilibrium nature of the environment likely affects the rate of power generation, but not significantly the maximum power achievable in the steady state. Efficiency, in contrast to power, shows a more complex relationship with the ratios. Although efficiency generally increases, there is a clear optimum for each. Increasing excessively reduces efficiency. This indicates an optimal energy level difference for maximum efficiency in a non-equilibrium setting; exceeding this optimum leads to energy losses due to non-ideal processes dominating work extraction [30,40]. This effect is likely amplified in a non-equilibrium system where energy dissipation processes are more prevalent.

HCOP has relatively low across the examined quantum otto engines operations. The HCOP shows a slight increase T_h/T_c but has a more complex, non-monotonic relationship, suggesting trade-offs between thermal management and power generation in the non-equilibrium environment. Similar to HCOP, the CCOP is also relatively low, confirming the engine's dominance. It displays a more significant increase between CCOP.

In examining the long-term behavior of the single-qubit Otto cycle, we derive an explicit analytic expression for its power output once the system is far from a steady state. In the numerical analysis, the reference energy scale is set by normalizing ω_c to a maximum of 1 , with $\omega_c \leq 1$. The cold bath temperature is chosen to be $T_c \leq 5$ to enable consistent comparisons across different parameter values. Transition rates for both heat reservoirs are kept equal at $\kappa_h = \kappa_c \leq \kappa$, and the durations of interaction with each bath are fixed at $t_h = t_c = 50$.The amount of heat transferred during each phase depends on the chosen parameters. Modulating the higher energy level ω_h and the temperature of the hot reservoir T_h causes the system's operational mode to vary according to their ratios.

In the work mode, the cycle's efficiency η and power P are primarily dictated by the ratio ω_h/ω_c and the temperature differential T_h/T_c, illustrating how these parameters govern the thermodynamic performance of the quantum otto engine. The power as a function of these ratios typically exhibits a distinct maximum, which was characterized by analyzing the ratio ω_h/ω_c.

In the context of the non-equilibrium nature of the environment, it is implicitly represented in the model parameters and how they influence the results. Unlike in an ideal equilibrium setting, the heat transfer and work extraction processes are not perfect. Energy losses due to various irreversibilities (which are more pronounced in non-equilibrium) are implicitly accounted for in the calculated power and efficiency, resulting in lower values compared to what you would expect from an ideal Otto cycle model [29,41]. The complex and non-monotonic relationships between the performance metrics highlight the interplay of irreversible processes affecting the engine’s performance. The optima observed in efficiency suggest that there exists an optimal operation point for maximizing work extraction while minimizing energy losses due to non-equilibrium effects.

2 Discussion

This study provides an analysis of quantum Otto heat engines operating in non-equilibrium, offering valuable insights into the fundamental thermodynamic principles governing these systems. The analysis of both individual and interacting qubit systems demonstrates how quantum effects—like coherence and entanglement interact with practical constraints such as temperature differences, external influences, environmental disturbances, and loss of quantum coherence, shaping their thermal performance and operational efficiency [42].

The numerical simulations demonstrate that non-equilibrium effects can significantly reduce the efficiency of quantum Otto engines compared to idealized scenarios. This finding underscores the importance of considering both quantum mechanical properties and practical constraints in the design and optimization of these engines. Specifically, the analysis highlights the trade-offs between power, efficiency, and performance coefficients, emphasizing the influence of temperature differences and internal coupling strength. The observation of an optimal energy level difference (ω_h/ω_c) for maximizing efficiency in non-equilibrium settings suggests that careful tuning of engine parameters is crucial for achieving optimal performance [43].

Furthermore, the comparison of classical and quantum Otto cycle efficiencies under both equilibrium and non-equilibrium conditions reveals the potential advantages and limitations of quantum engines. While quantum effects may offer pathways for improved efficiency, the presence of non-equilibrium factors can significantly diminish these benefits, leading to efficiencies lower than the theoretical Carnot limit. This highlights the need for strategies to mitigate the detrimental effects of irreversibilities and energy dissipation processes in practical quantum heat engine implementations.

2.1 Implications and Future Directions

The detailed modeling underscores that non-equilibrium environments can be exploited to surpass classical bounds, but they also pose challenges through increased irreversibility. Coherent control, reservoir engineering, and system-bath spectral tailoring emerge as promising tools to optimize performance. Moreover, understanding the interplay between quantum coherence and dissipation remains pivotal for practical implementation.

Advancing the theoretical framework involves integrating quantum information concepts, such as entanglement and quantum correlations, with thermodynamic principles. Experimentally, realizing such engines demands sophisticated control over quantum systems and environments, leveraging platforms like superconducting qubits, trapped ions, or quantum dots.

Conclusion

In conclusion, this research contributes to the growing body of knowledge in quantum thermodynamics by providing a detailed analysis of quantum Otto heat engines in non-equilibrium environments. The findings demonstrate that while quantum effects offer the potential for enhanced engine performance, the presence of non-equilibrium conditions poses significant challenges to achieving optimal efficiency. The study emphasizes the importance of considering both quantum mechanical properties and real-world limitations in the design and optimization of quantum heat engines for applications in quantum computing, sustainable energy technologies, and thermodynamic cycles at the quantum scale.

Future research should focus on developing strategies to mitigate the detrimental effects of non-equilibrium factors, such as noise and decoherence, and to enhance the robustness of quantum Otto engines in practical settings. Further investigation into the role of quantum coherence and entanglement in improving engine performance under non-equilibrium conditions is also warranted. Additionally, exploring novel materials and architectures for quantum heat engines may lead to the development of more efficient and robust devices for energy conversion and quantum information processing. Finally, experimental validation of the theoretical predictions presented in this study is crucial for advancing the field of quantum thermodynamics and realizing the full potential of quantum heat engines.

References

[1] Alicki, R. & Kosloff, R. The open system and the second law of thermodynamics. *New J. Phys.* **20**, 015008 (2018).

[2] Alipour, S. *et al.* Correlations in quantum thermodynamics: Heat, work, and entropy production. *Sci. Rep.* **6**, 35568 (2016).

[3] Bouton, Q. *et al.* A quantum heat engine driven by atomic collisions. *Nat. Commun.* **12**, 2063 (2021).

[4] Cangemi, L. M., Bhadra, C. & Levy, A. Quantum engines and refrigerators. *Phys. Rep.* **1087**, 1–71 (2024).

[5] Gao, J. & Hatano, N. Maximum power of coupled-qubit otto engines. *Phys. Rev. Res.* **6**, 023172 (2024).

[6] Goold, J., Hovhannisyan, K. V., Nourmandipour, A. & Perarnau-Llobet, M. From quantum to classical thermodynamics: The otto cycle. *Nat. Commun.* **7**, 12493 (2016).

[7] Hovhannisyan, V. Single-qubit quantum otto engine. *Phys. Rev. Lett.* **111**, 070402 (2013).

[8] Jevtic, S., Newman, D., Rudolph, T. & Stace, T. M. Single-qubit thermometry. *Phys. Rev. A* **91**, 012331 (2015).

[9] Linden, N., Popescu, S., Short, A. & Winter, W. Thermodynamic efficiency of one- and two-qubit engines. *Phys. Rev. Lett.* **101**, 130401 (2010).

[10] Linden, N. Quantum mechanical examples of non-equilibrium thermodynamics. *J. Phys. Math. Theor.* **43**, 195304 (2010).

[11] Manzano, G. & Zambrini, R. Quantum thermodynamics under continuous monitoring: A general framework. *AVS Quantum Sci.* **4**, (2022).

[12] Maruyama, K., Nakamura, T. & Saito, K. Colloquium: The physics of quantum thermodynamics. *Rev. Mod. Phys.* **81**, 1 (2009).

[13] Mitchison, M. T. & Kwiat, P. G. Non-equilibrium quantum otto engine. *Phys. Rev. Res.* **1**, 033082 (2019).

[14] Linpeng, X. *et al.* Energetic cost of measurements using quantum, coherent, and thermal light. *Phys. Rev. Lett.* **128**, 220506 (2022).

[15] Lisboa, V. F., Dieguez, P. R., Guimarães, J. R., Santos, J. F. G. & Serra, R. M. Experimental investigation of a quantum heat engine powered by generalized measurements. *Phys. Rev. A* **106**, 022436 (2022).

[16] Son, J., Talkner, P. & Thingna, J. Charging quantum batteries via otto machines: Influence of monitoring. *Phys. Rev. A* **106**, 052202 (2022).

[17] Son, J., Talkner, P. & Thingna, J. Monitoring quantum otto engines. *PRX Quantum* **2**, 040328 (2021).

[18] Ding, X., Yi, J., Kim, Y. W. & Talkner, P. Measurement-driven single temperature engine. *Phys. Rev. E* **98**, 042122 (2018).

[19] Zheng, Y., Hänggi, P. & Poletti, D. Occurrence of discontinuities in the performance of finite-time quantum otto cycles. *Phys. Rev. E* **94**, 012137 (2016).

[20] Zheng, Y. & Poletti, D. Quantum statistics and the performance of engine cycles. *Phys. Rev. E* **92**, 012110 (2015).

[21] Alhambra, A. M., Masanes, L., Oppenheim, J. & Perry, C. Fluctuating work: From quantum thermodynamical identities to a second law equality. *Phys. Rev. X* **6**, 041017 (2016).

[22] Abiuso, P. & Perarnau-Llobet, M. Optimal cycles for low-dissipation heat engines. *Phys. Rev. Lett.* **124**, 110606 (2020).

[23] Perarnau-Llobet, M. & Hovhannisyan, K. V. Quantum heat engines: A perspective on working substances. *Entropy* **17**, 7750–7768 (2015).

[24] Denzler, T. & Lutz, E. Power fluctuations in a finite-time quantum carnot engine. *Phys. Rev. Res.* **3**, 032041 (2021).

[25] Ng, N. H. Y., Woods, M. P. & Wehner, S. Surpassing the carnot efficiency by extracting imperfect work. *New J. Phys.* **19**, 113005 (2017).

[26] Campisi, M. & Fazio, R. The power of a critical heat engine. *Nat. Commun.* **7**, 11895 (2016).

[27] Watanabe, G. & Matsumoto, K. Efficiency of quantum otto engines with a finite number of particles. *Phys. Rev. E* **99**, 022117 (2019).

[28] Uzdin, R., Levy, A. & Kosloff, R. Equivalence of quantum heat machines, and quantum-thermodynamic signatures. *Phys. Rev. X* **5**, 031044 (2015).

[29] Verley, G., Esposito, M., Willaert, T. & Van den Broeck, C. The unlikely carnot efficiency. *Nat. Commun.* **5**, 4721 (2014).

[30] Pietzonka, P. & Seifert, U. Universal trade-off between power, efficiency, and constancy in steady-state heat engines. *Phys. Rev. Lett.* **120**, 190602 (2018).

[31] Klaers, J., Faelt, S., Imamoglu, A. & Togan, E. Squeezed thermal reservoirs as a resource for a nanomechanical engine beyond the carnot limit. *Phys. Rev. X* **7**, 031044 (2017).

[32] Sagawa, T. Thermodynamics of information processing in small systems. *Prog. Theor. Phys.* **127**, 1–56 (2012).

[33] Horodecki, M. & Oppenheim, J. Fundamental limitations for quantum and nanoscale thermodynamics. *Nat. Commun.* **4**, 2059 (2013).

[34] Guo, J., Wang, J., Wang, Y. & Chen, J. Universal efficiency bounds of weak-dissipative thermodynamic cycles at the maximum power output. *Phys. Rev. E* **87**, 012133 (2013).

[35] Kosloff, R. & Levy, A. Quantum heat engines and refrigerators: Continuous devices. *Annu. Rev. Phys. Chem.* **65**, 365 (2014).

[36] Ma, Y.-H., Xu, D., Dong, H. & Sun, C.-P. Universal constraint for efficiency and power of a low-dissipation heat engine. *Phys. Rev. E* **98**, 042112 (2018).

[37] Manikandan, S. K., Dabelow, L., Eichhorn, R. & Krishnamurthy, S. Efficiency fluctuations in microscopic machines. *Phys. Rev. Lett.* **122**, 140601 (2019).
[38] Cavina, V. Thermodynamics of open quantum systems: from a critical study to the optimization of non-equilibrium heat engines. *IRIS* (2019).
[39] Brandner, K. & Saito, K. Thermodynamic geometry of microscopic heat engines. *Phys. Rev. Lett.* **124**, 040602 (2020).
[40] Dorfman, K. E., Xu, D. & Cao, J. Efficiency at maximum power of a laser quantum heat engine enhanced by noise-induced coherence. *Phys. Rev. E* **97**, 042120 (2018).
[41] Singh, V. Optimal operation of a three-level quantum heat engine and universal nature of efficiency. *Phys. Rev. Res.* **2**, 043187 (2020).
[42] Miller, H. J. D. & Mehboudi, M. Geometry of work fluctuations versus efficiency in microscopic thermal machines. *Phys. Rev. Lett.* **125**, 260602 (2020).
[43] Skrzypczyk, P., Short, A. J. & Popescu, S. Work extraction and thermodynamics for individual quantum systems. *Nat. Commun.* **5**, 4185 (2014).